Available online at www.sciencedirect.com
SCIENCE DIRECT®
Journal of Catalysis 220 (2003) 115–126
JOURNAL OF CATALYSIS
www.elsevier.com/locate/jcat

Influence of Sn additives on the selectivity of hydrogenation of α-β-unsaturated aldehydes with Pt catalysts: a density functional study of molecular adsorption

F. Delbecq [a,*] and P. Sautet [b]

[a] *Institut de Recherches sur la Catalyse, 2 Avenue Albert Einstein, F-69626 Villeurbanne cedex, France*
[b] *Laboratoire de Chimie, UMR CNRS, Ecole Normale Supérieure de Lyon, 46 Allée d'Italie, F-69364 Lyon cedex 07, France*

Received 13 February 2003; revised 26 May 2003; accepted 26 May 2003

Abstract

In this study, the adsorption and the reactive properties of α-β-unsaturated aldehydes are studied by means of density functional calculations (DFT) on two well-defined Pt–Sn alloy surfaces, p(2 × 2) Pt_3Sn(111) and $(\sqrt{3} \times \sqrt{3})R30°$ Pt_2Sn(111). First the electronic structure of the bulk alloys is determined: a charge transfer occurs from Sn to Pt, the work function decreases, and the d-band center is shifted away from the Fermi level. Then various adsorption structures of acrolein (propenal), crotonaldehyde (2-butenal), and prenal (3-methyl, 2-butenal) are considered on the two alloys. The results are compared with those obtained on Pt(111). A large decrease of the adsorption energies is observed for the alloys. For acrolein, there is almost no change in the best adsorption modes, the adsorption through the C=C bond being predominant. This explains why the selectivity of the acrolein hydrogenation is not changed much when Pt–Sn alloys and Pt are compared. For prenal on the contrary, only the atop mode is stable on the alloys, whereas a structure parallel to the surface is the most stable one on Pt. This explains the modified reaction selectivity with a larger amount of unsaturated alcohol in the products in the case of the Sn alloys.

Keywords: Unsaturated aldehydes; Adsorption; Hydrogenation; DFT calculations; Pt–Sn alloys; Selectivity; Acrolein; Crotonaldehyde; Prenal

1. Introduction

The alloys of tin with transition metals have been widely used during the last decade in order to improve the catalytic properties of these metals. Particularly, the alloys of tin with platinum have been shown to greatly enhance the selectivity of the hydrogenation of the α-β-unsaturated aldehydes. Effectively, compared to pure Pt, the yield in unsaturated alcohol, a product showing interesting properties in the fine chemical industry, is increased [1–11]. The origin of this catalytic effect in not totally understood and several hypotheses exist: Sn can act as an inert, site-blocking agent that changes the adsorption site of the molecules, and Sn can induce electronic effects on Pt, modifying its adsorption properties.

The chemisorptive properties of the Pt/Sn alloys have been studied with several kinds of adsorbates like CO [12,13], NO [14], and alkenes [15–17]. In all cases, the adsorption energy decreases on the alloys compared with pure platinum. It has also been shown that alkenes keep the same adsorption geometry (di-σ) on the alloys. No experimental data exist concerning the adsorption of aldehydes or ketones on the Pt/Sn alloys.

α-β-Unsaturated aldehydes like acrolein, crotonaldehyde (2-butenal), or prenal (3-methyl 2-butenal) contain a C=C and a C=O double bonds in conjugation. Both double bonds can be hydrogenated following Scheme 1. Hydrogenation of the C=C bond gives a saturated aldehyde SAL, that of the C=O bond gives an unsaturated alcohol UOL. Both SAL and UOL can be further hydrogenated in saturated alcohol SOL. The selectivity of the hydrogenation depends on the double bond which is hydrogenated preferentially. The knowledge of their adsorption modes can help to understand their reactivity, although this is not the only important factor. Indeed the coadsorption of hydrogen can also play a role. Moreover the most active species for hydrogenation is not necessarily the most stable one, as it has been observed in the case of ethylene [18]. We have already studied the ad-

* Corresponding author.
E-mail address: delbecq@catalyse.univ-lyon1.fr (F. Delbecq).

0021-9517/$ – see front matter
doi:10.1016/S0021-9517(03)00249-5

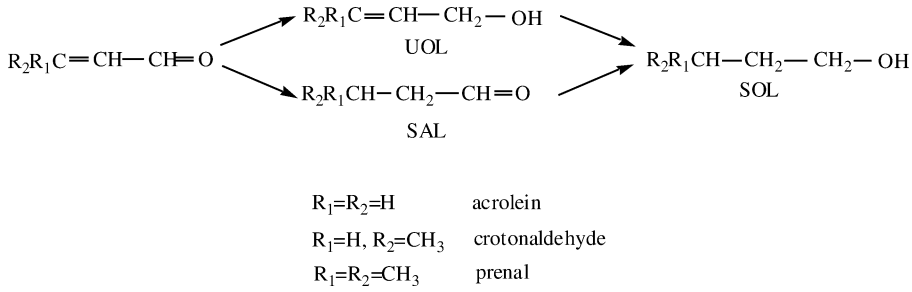

Scheme 1. Possible products obtained by hydrogenation of α-β-unsaturated aldehydes.

sorption modes of these aldehydes on platinum by means of DFT periodic calculations [19] and our purpose in this work is to present our results for a similar study on two Pt/Sn alloys.

Few theoretical works deal with calculations on these alloys. We can cite a study of the electronic structure [20] and studies of adsorption properties: CO [21], H_2S and S_2 [22], SO_2 [23], and ethylene [24,25]. In most of these calculations, the surfaces are modeled by clusters, except the last one [25].

By vapor deposition of Sn on platinum, followed by annealing, well-defined surface alloys are formed. The structure of these alloys has been experimentally determined for the three faces of the fcc crystal: 110 [26], 100 [27,28], and 111 [27,29–32]. Only the latter has been considered in the present study. When several monolayers of Sn are evaporated onto a Pt(111) crystal and then annealed, two surface structures are formed depending on the Sn coverage: either a p(2 × 2) or a $(\sqrt{3} \times \sqrt{3})R30°$ Sn/Pt(111) structure as observed by LEED [29] with stoichiometry Pt_3Sn and Pt_2Sn, respectively. It has been shown by XPD that these surfaces consist in a single alloy layer on pure platinum [32]. Both surfaces exhibit a slight buckling in which Sn protrudes about 0.22 Å above the first Pt layer [30]. Another LEED result gives an outward displacement of Sn atoms of 0.30 and 0.23 Å for the (2 × 2) and $(\sqrt{3} \times \sqrt{3})R30°$ phase, respectively [31].

The ordered structure of these two Sn/Pt(111) alloys is well adapted to the use of periodic methods for their study. We will first study the geometrical and electronic structures of the bare alloys, then we will consider the adsorption modes of acrolein, crotonaldehyde, and prenal on the $(\sqrt{3} \times \sqrt{3})R30°$ surface and those of acrolein and prenal on the (2 × 2) surface. Finally, the implications for the selective hydrogenation of these molecules will be discussed.

2. Computational method

The calculations were performed with the Vienna ab initio simulation program (VASP) [33–35]. This program performs density functional theory calculations using a plane-wave basis set and ultrasoft pseudo-potentials (for Sn 14 valence electrons are considered). The generalized gradient approximation (GGA) level was used with the functional of Perdew and Wang 91 [36].

The surface alloy was modeled by a periodic four-layer slab, with adsorption on one side of the slab. Only the first layer contains Sn atoms in a stoichiometry Pt_3Sn for the (2 × 2) structure and Pt_2Sn for the $(\sqrt{3} \times \sqrt{3})R30°$ one. Each slab is separated from its periodic image in the z direction by a vacuum space corresponding to four layers (eight layers in the case of atop adsorption). For all structures, the geometry optimization included all degrees of freedom of the adsorbates and of the two uppermost metal layers. Most of the calculations were done with unit cells containing 9 atoms per layer for the $(\sqrt{3} \times \sqrt{3})R30°$ surface and 12 atoms per layer for the (2 × 2) surface. The lattice vectors were therefore 3 × 3 for the former surface and $2\sqrt{3} \times 2\sqrt{3}$ for the latter. This is illustrated on Fig. 1. One molecule is adsorbed per unit cell, which gives a coverage $\theta = 1/9$ and

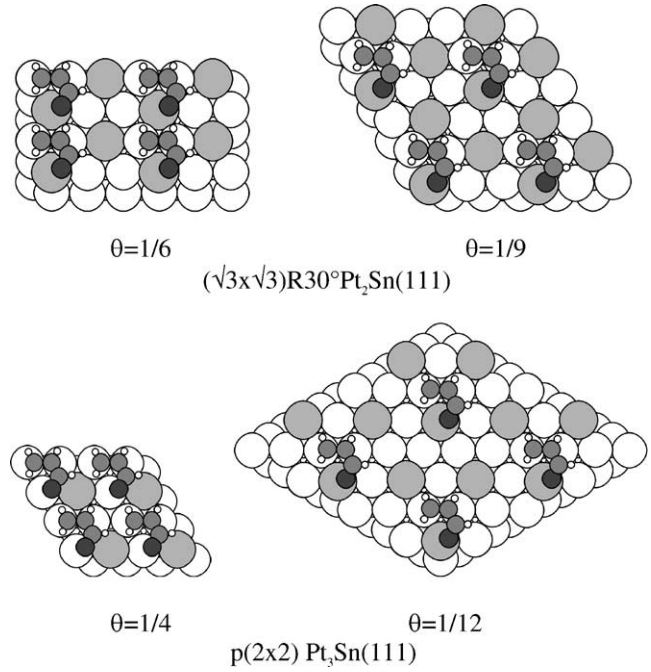

Fig. 1. Surfaces of the $(\sqrt{3} \times \sqrt{3})R30°$ $Pt_2Sn(111)$ alloy (top) and of the p(2 × 2) Pt_3Sn alloy (bottom) with a molecular coverage of 1/6 and 1/9 and 1/4 and 1/12, respectively. The example of a di-σ_{CC} adsorption of acrolein is shown (Pt, large white; Sn, large gray; C, medium grey; O, medium black; H, small white). The periodicity of the molecules indicates the unit cell ($3 \times \sqrt{3}$, 3 × 3, 2 × 2, and $2\sqrt{3} \times 2\sqrt{3}$, respectively).

1/12, respectively. Higher coverages were also considered in the case of acrolein: 1/6 for the Pt_2Sn alloy (lattice vector 3×2) and 1/4 for the Pt_3Sn alloy (lattice vector $\sqrt{3} \times \sqrt{3}$). The Brillouin zone integration was done on a $3 \times 3 \times 1$ grid for coverages 1/9 and 1/12, on a $3 \times 5 \times 1$ grid for coverage 1/6, and $5 \times 5 \times 1$ for coverage 1/4.

The same metal interatomic distance (2.82 Å) as in the case of pure platinum was used for the frozen part of the slab (optimized from Pt bulk calculations, 2% larger than the experimental value 2.77 Å). This is justified by the fact that experimentally the lattice parameter is imposed by the underlying Pt bulk, and the Sn atoms in the uppermost layer accommodate this constraint by an outward displacement, inducing a Pt–Sn distance of 2.86 Å. The adsorption energy is defined as the difference between the energy of the whole system and that of the bare slab and the isolated adsorbate.

Since the molecules are adsorbed on one side of the slab only, the unit cell has a net dipole and a spurious electrostatic interaction between the slab and its periodic images can modify the total energy. This effect could be important in the case of polarizable molecules like unsaturated aldehydes, particularly for the vertical adsorption modes. A correction has been applied both on the energy and on the potential, in order to remove this effect. For the planar adsorption modes, the correction does not exceed 1 kcal/mol for acrolein and 2 kcal/mol for prenal showing that a four-layer thick vacuum is sufficient. For the vertical adsorption modes, the correction is as high as 6 kcal/mol for prenal, hence a five-layer vacuum is not enough if no correction is applied. Even with a eight-layer vacuum, there is still a correction of 1 kcal/mol due to the dipole interactions. However the corrected values with a five- and eight-layer vacuum are the same, which shows that the use of a five-layer vacuum is sufficient if the dipole correction is done.

3. Structure of the alloys

The geometry of the slabs with the two different surface alloys was optimized. For the $(\sqrt{3} \times \sqrt{3})R30°$ structure, the Sn atoms were found to be displaced outward by 0.23 Å for a calculation with five vacuum layers. For the (2×2) structure the displacement of the Sn atoms was 0.27 Å. These values are in good agreement with the experimental ones.

The work functions have been calculated to be 5.4 and 5.3 eV for the $p(2 \times 2)$ and the $(\sqrt{3} \times \sqrt{3})R30°$ alloys, respectively. This shows a decrease compared with pure platinum work function for which the calculations give 5.7 eV. These results are similar to those obtained by other calculations [25] and compare well with the experimental values, 5.8 eV for Pt(111), 5.4 eV for $p(2 \times 2)$ $Pt_3Sn(111)$, and 5.2 eV for $(\sqrt{3} \times \sqrt{3})R30°$ $Pt_2Sn(111)$ [12].

To analyze the electronic structure of these surfaces, we have performed calculations with the ADF-Band program. This code, based on atomic orbitals and not on plane waves, allows us to obtain the electronic populations by a Mulliken analysis. The calculations were done with the geometries determined previously by VASP. They include a scalar relativistic effect, necessary for treating platinum. Three layers were considered. The unit cell contained three atoms (Pt_2Sn) for the $(\sqrt{3} \times \sqrt{3})R30°$ surface and four atoms (Pt_3Sn) for the (2×2) one. These calculations showed a charge transfer from Sn to Pt, in agreement with the relative electronegativities of the atoms (2.2 and 1.8 for Pt and Sn, respectively, following Pauling's scale, 5.6 and 4.3, respectively, following Pearson scale [37]) and with previous works performed with clusters [22,24]. In the case of the $(\sqrt{3} \times \sqrt{3})R30°$ surface, the Sn atoms lose 0.42 e^- and the surface Pt atoms gain 0.13 e^-. For the $p(2 \times 2)$ surface, the Sn atoms lose more (0.53 e^-) and the Pt atoms gain less (0.10 e^-). A similar transfer has been found in the case of cluster calculations [24]. As a reference, a calculation was also done for a three-layer slab of pure platinum. In this case, the surface atoms bare a positive charge of +0.06. That means that the surface Pt atoms are more negatively charged for the alloys than for pure platinum. For both alloys, the d orbitals gain the largest part of the transferred charge (0.2 and 0.1 e^- for the $(\sqrt{3} \times \sqrt{3})R30°$ and the (2×2), respectively).

The density of states (DOS) projected on a surface Pt atom for Pt(111) and the two alloys are compared on Fig. 2. The d-band is narrower in the case of the alloys. One observes a different shape around the Fermi level (E_F): in the case of Pt(111), there is a large density of states just at E_F, which is smaller in the case of Pt_3Sn and disappears for Pt_2Sn, in agreement with UPS spectra [12]. Furthermore, the d-band center relative to the corresponding Fermi level is calculated at −1.93 eV for Pt(111), −2.09 eV for the $p(2 \times 2)$ Pt_3Sn alloy, and −2.12 eV for the $(\sqrt{3} \times \sqrt{3})R30°$ Pt_2Sn alloy. Hence the d-band center goes down when platinum is alloyed with tin, which is consistent with the interaction with a more electropositive metal. The greater density of states around E_F observed for Pt_3Sn compared to Pt_2Sn could explain why the Pt atoms appear brighter for the $p(2 \times 2)$ alloy than for the $(\sqrt{3} \times \sqrt{3})R30°$ one in the STM images [38].

4. Adsorption of acrolein, crotonaldehyde, and prenal on the $(\sqrt{3} \times \sqrt{3})R30°$ Sn/Pt(111) surface

In this section, the adsorption of the three aldehydes will be compared on the $(\sqrt{3} \times \sqrt{3})R30°$ surface alloy, at coverage $\theta = 1/9$ first. A comparison will also be done with the adsorption of the same aldehydes on pure platinum [19]. The possible adsorption structures of α-β-unsaturated aldehydes are numerous since each double bond can interact with the surface in several configurations. Their number is even increased for the alloy, compared with pure Pt, since the surface atoms involved in the adsorption can be either Pt or Sn. These structures are shown on Fig. 3. They all have been tested and only the most stable ones will be given here. For example, it appeared that the C=C bond did not adsorb fa-

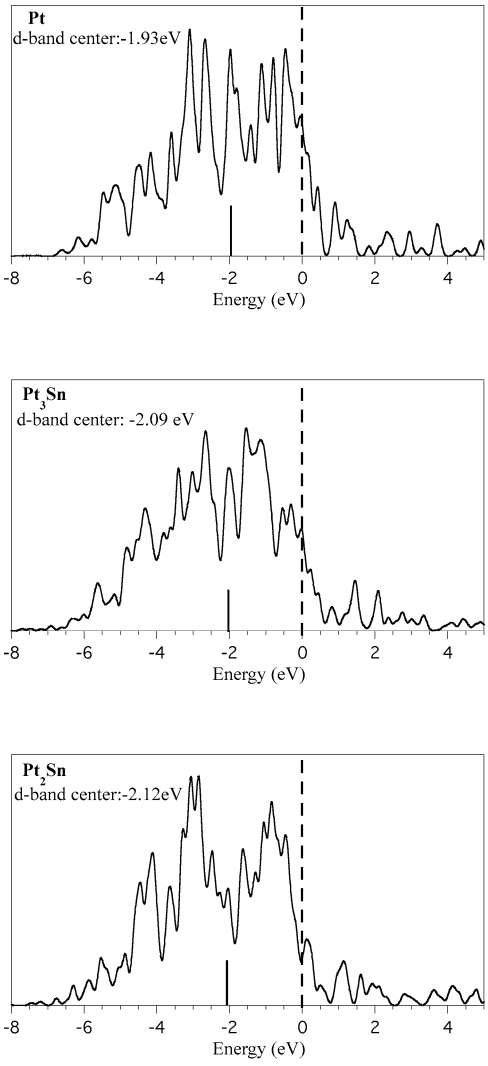

Fig. 2. DOS (density of states) projected on a surface Pt atom in the case of pure platinum, of the p(2 × 2) Pt_3Sn alloy, and of the $(\sqrt{3} \times \sqrt{3})R30°$ Pt_2Sn alloy. The dashed line indicates the Fermi level and the vertical segment shows the energy center of the d-band.

vorably on a site containing a Sn atom, which excludes some geometries like the η_4Sn *trans* one, the equivalent of which was one of the most stable cases on Pt(111) (the Sn term in the name of an adsorption structure indicates that the oxygen atom interacts with a tin atom). For acrolein finally, only seven of them have significant adsorption energies. Two involve both the C=C double bond and the oxygen atom: the η_3-Sn *cis* and the η_3-Sn *trans* where the C=C bond adsorbs on two Pt atoms and the oxygen binds to a Sn atom. The equivalent geometry exists on pure Pt [19] and involves a Pt–O interaction. The geometry where the two double bonds interact with the surface (η_4-Sn *cis* $= \pi_{CC} +$ di-σ_{CO}), in such a way that the C=O bond is bound to a Sn atom, transforms into the η_3-Sn *cis* geometry whereas it exists on Pt(111). The η_4-Sn *trans* (di-σ_{CC} + di-σ_{CO}) which also exists on Pt(111) cannot exist on this alloy because a Sn atom would be involved in the adsorption of the C=C bond. The η_4 *cis*

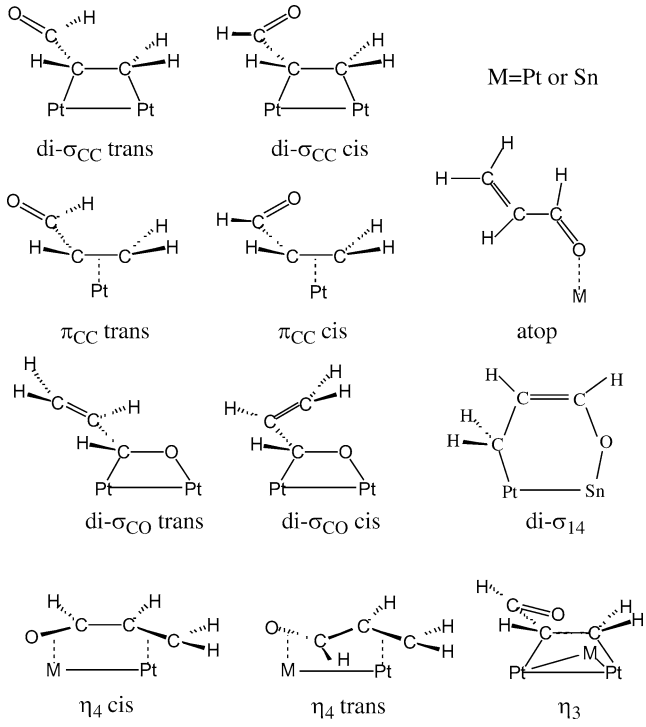

Fig. 3. Schematic description of the various possible adsorption modes considered for each molecule.

mode adsorbed only on Pt atoms evolves to a π_{CC} *cis* geometry. Three other geometries only involve the C=C bond, the di-σ_{CC} *trans* and the π_{CC} *cis* and *trans*. The di-σ_{CC} *cis* mode, which exists on pure Pt, does not exist here as a stable minimum but transforms into the η_3Sn *cis* mode with a Sn–O interaction. Effectively, this interaction is, as expected, stronger than the Pt–O one.

A structure that does not exist on pure Pt appears on the alloy: the di-σ_{14} geometry where only the two extremities of the molecule interact with the surface in a kind of metallacycle (Fig. 3). Such a structure has been postulated to explain the 1-4 hydrogenation of butadiene, for example. The last structure is an atop geometry where the oxygen atom interacts with a Sn atom (atop-Sn). The di-σ_{CO} mode has also been considered. This mode has been found weakly bound on Pt(111), less than the atop-Pt one, as expected for a substituted aldehyde. Nevertheless, the presence of tin could modify its stability. We have thus tried a di-σ_{CO} geometry with the oxygen atom bound to a Sn atom. Such a structure is not stable for acrolein and it evolves into the atop-Sn geometry for prenal. The atop-Pt mode, where the oxygen atom is bound to a platinum, has also been calculated. It is not stable on the surface.

For crotonaldehyde and prenal, the same adsorption geometries are found and moreover another mode exists, the η_4Sn *cis* one. In this mode, both double bonds interact with the surface, giving a planar adsorption geometry. An equivalent mode exists also on Pt(111). For acrolein, this mode does not exist and evolves during optimization to the η_3Sn *cis* mode (Table 2).

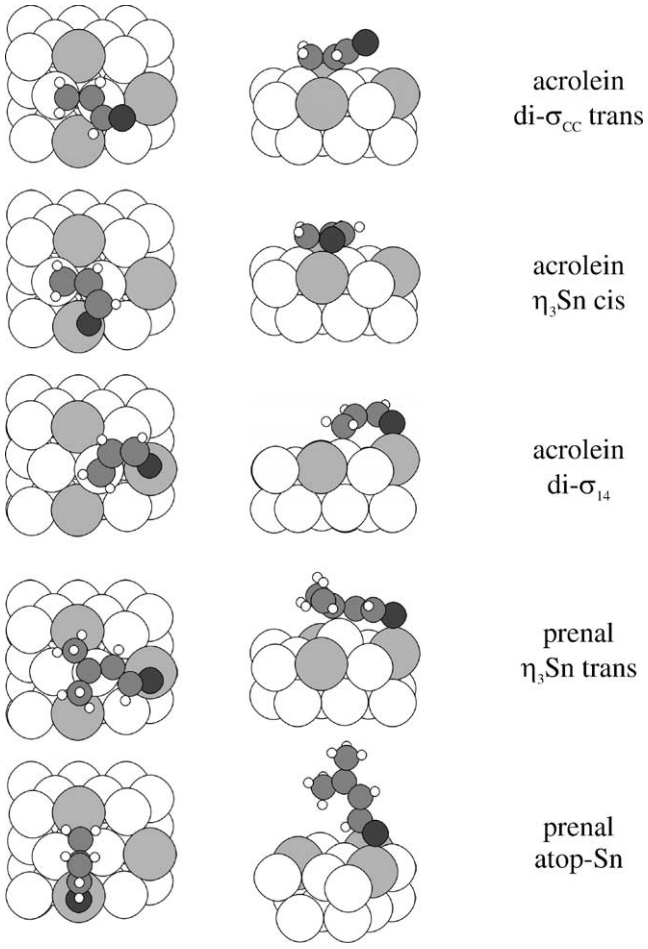

Fig. 4. Top and side views of the most stable adsorption modes of acrolein and prenal on the $(\sqrt{3}\times\sqrt{3})R30^\circ$ Pt_2Sn alloy (see Fig. 1 for labels of spheres).

The most stable modes for acrolein and prenal are described in Fig. 4. One can note the important difference between the di-σ_{CC} mode where the C=O bond moves out of the surface and the η_3 modes where the molecule lies parallel to the surface. The η_3Sn *cis* mode is a di-σ_{CC} mode with an interaction of the oxygen with the surface while the η_3Sn *trans* one is a π_{CC} mode with the same O interaction. For the di-σ_{14} geometry, the medium carbon atoms are clearly far from the surface. The metal atoms involved in the adsorption are pulled out of the surface and protrude largely. This can be observed in Fig. 4, particularly for the di-σ_{14} mode of acrolein and the η_3Sn *trans* mode of prenal. In the case of acrolein, for example, the buckling of the Sn atom is 0.25 Å for η_3Sn *cis* and *trans* and 0.48 Å for di-σ_{14} relative to the noninteracting tin atoms. The buckling of the Pt atom is 0.4 Å for η_3Sn *cis*, 0.5 Å for di-σ_{14}, and as much as 0.95 Å for η_3Sn *trans*. For prenal in the η_3Sn *trans* mode, the buckling of Sn is 0.24 Å and that of Pt 1.1 Å. The displacement of the metal atoms involved in the adsorption is a general phenomenon. Since new bonds are created, such atoms fill their coordination sphere and are hence less strongly bound to the other metal atoms, which induces a lengthening of the metal–metal bonds with the second layer. This is a consequence of the bond order conservation principle. The stronger the adsorption, the greater the displacement. Moreover in the η_3Sn *trans* mode where the C=C bond is π bonded to one Pt atom, two new bonds are formed for this atom, which explains its huge buckling.

Table 1
Most important geometrical parameters for the adsorption structures of acrolein on $(\sqrt{3}\times\sqrt{3})R30^\circ$ Sn/Pt(111) (in Å) for $\theta = 1/9$

	PtC_1	PtC_2	PtC_3	SnO	C_1C_2	C_2C_3	C_3O
di-σ_{CC} *trans*	2.14	2.18			1.48	1.48	1.23
π_{CC} *trans*	2.18	2.24			1.41	1.47	1.23
π_{CC} *cis*	2.18	2.25			1.42	1.48	1.23
di-σ_{14}	2.18			2.17	1.43	1.38	1.31
η_3Sn *cis*	2.13	2.27	2.67	2.33	1.47	1.43	1.28
η_3Sn *trans*	2.15	2.26	2.97	2.45	1.42	1.44	1.26
Atop-Sn				2.42	1.34	1.45	1.24

The numbering of the atoms is as follows: C_1=C_2–C_3=O.

Table 2
Adsorption modes and binding energies (in kcal/mol) of acrolein, crotonaldehyde, and prenal on $(\sqrt{3}\times\sqrt{3})R30^\circ$ Sn/Pt(111)

θ	Acrolein		Crotonaldehyde		Prenal
	1/6	1/9	1/6	1/9	1/9
di-σ_{CC} *trans*	−8.7	−11.1	−3.2	−6.0	−0.6
di-σ_{CC} *cis*	−12.0	η_3Sn *cis*	−5.8		
π_{CC} *trans*	−6.3	−8.7		−5.3	−0.9
π_{CC} *cis*	−9.0	−5.4			
di-σ_{14}	−12.8	−13.8	−5.8	−7.4	−0.7
η_3Sn *cis*[a]	di-σ_{CC} *cis*	−15.8	η_4Sn *cis*	−9.9	−2.7
η_3Sn *trans*[a]	π_{CC} *trans*	−9.3		−6.2	−3.9
η_4Sn *cis*[a]	di-σ_{CC} *cis*	η_3Sn *cis*	−3.1	−6.0	−0.2
Atop-Sn[a,b]	−3.7	−3.0	−3.7	−5.0	−6.6

[a] The Sn term means that the oxygen atom interacts with a tin atom.
[b] With 8 layers of vacuum between slabs.

The main bond lengths for these various modes are given in Table 1 in the case of acrolein. As we have already observed in the case of the adsorption on Pt(111) [19], the bonds are elongated when they interact with the surface: 1.48 Å for the C=C bond (1.34 for gaseous acrolein), and 1.26–1.31 Å for the C=O bond (1.23 for gaseous acrolein). The Pt–C bonds are all in the range 2.13–2.27 Å which corresponds to usual lengths in platinum complexes. The bond lengths are identical to those found on Pt(111), which shows that the Pt–C interaction has a similar nature on the pure metal and on the alloy. This similarity has been pointed out experimentally in the case of the adsorption of ethylene [15]. Let us comment with more detail the di-σ_{14} geometry: the Pt–C bond (2.176 Å) and the Pt–O bond (2.17 Å) are short and real single bonds. The C_1C_2 bond (1.43 Å) is intermediate between a single and a double bond and the C_3–O bond (1.31 Å) is elongated compared to its value in gaseous acrolein. On the contrary, the C_2C_3 bond (1.38 Å) is shortened and is close to a double bond. These lengths correspond to the structure given on Fig. 3.

The energetic results are given in Table 2. The most stable mode for acrolein is the η_3Sn *cis* one followed by di-σ_{14},

the di-σ_{CC} being less stable. When the adsorption of crotonaldehyde and prenal is compared to that of acrolein, the same trend is observed as in the case of the adsorption on Pt(111): there is a decrease in the adsorption energy when going from acrolein to crotonaldehyde and to prenal. This decrease is mainly due to the repulsive steric effect of the methyl groups. An exception is the atop-Sn mode which, on the contrary, becomes more stable when the C=C bond is substituted (from 3 to 6.6 kcal/mol). This is due to the electron–donor effect of the methyl groups transmitted by the conjugated chain, which induces a better interaction of the oxygen lone pair with the surface. The same behavior is observed for the atop-Pt mode on Pt(111). The best mode for crotonaldehyde is also η_3Sn *cis*, followed by di-σ_{14}. However the other modes are not far away, particularly the atop-Sn mode which is only 1 kcal/mol less stable than η_3Sn *trans* compared to 6 kcal/mol in the case of acrolein, as a result of the previously described trend. For prenal, only three modes can be considered as bound to the surface, although the binding energy is weak. Among them the atop-Sn is the most stable.

A consequence is that the preferred adsorption modes of the three aldehydes are very different. Acrolein prefers the η_3Sn *cis* mode and the second best geometry is the metallacycle di-σ_{14}. For crotonaldehyde, the η_3Sn *cis* mode is also the most stable but in tight competition with several other structures. Finally for prenal, the atop-Sn mode is the sole which has a significant adsorption energy, even more stable than for the two other aldehydes.

At higher coverage (1/6), the planar adsorption modes parallel to the surface (η_3 or η_4) do not exist anymore, because they take too much space on the surface, and the best adsorption mode for acrolein is the di-σ_{14} one. However, the di-σ_{CC} *cis* mode is close in energy and can be in competition. For prenal obviously, the adsorption mode remains atop-Sn at this coverage. The results are different on pure platinum for this coverage since the η_3 and η_4 modes of acrolein remain the most stable ones. The difference comes from the lattice vectors used for generating the surface. In the case of Pt_2Sn, the superlattice must be compatible with the periodicity of the Sn atoms, and hence the unit cell for a coverage of 1/6 is a rect$(3 \times \sqrt{3})$ lattice (see Fig. 1), where some intermolecular contacts are present for the planar structures. In the case of Pt, another lattice is possible (3×2) leading to this more favorable adsorption for the planar forms.

5. Adsorption of acrolein and prenal on the p(2 × 2) Sn/Pt(111) surface

In the case of the p(2 × 2) Pt_3Sn alloy, only acrolein and prenal have been considered. There are less Sn atoms on the surface, thus some geometries stable on Pt(111) and which do not exist on the $(\sqrt{3} \times \sqrt{3})R30°$ alloy are found on this alloy. This is the case of the η_3 *cis* and η_4 *cis* geometries where only Pt atoms are involved. This is also the case for the η_4Sn *trans* mode where the oxygen atom interacts with a Sn atom. Except for these modes, the other ones are the same as in the previous studied alloy and will not be described in detail.

Table 3
Adsorption modes and binding energies (in kcal/mol) of acrolein and prenal on p(2 × 2) Sn/Pt(111) at a coverage of $\theta = 1/12$

	Acrolein		Prenal
	1/4	1/12	1/12
di-σ_{CC} *trans*	−14.3	−12.4	Not stable
di-σ_{CC} *cis*	−14.7	−12.4	
di-σ_{14}	−12.4	−13.4	Not stable
η_3*cis*		−11.4	
η_4*cis*		−8.5	
η_3Sn *cis*[a]	−17.5[b]	−18.6	−4.0
η_3Sn *trans*[a]		−5.3	Not stable
η_4Sn *trans*[a]	−11.0	−15.5	−2.7
η_4Sn *cis*[a]	η_3Sn *cis*	−14.2	−3.9
Atop-Sn[a,c]	−4.5	−5.7	−7.7

[a] The Sn term means that the oxygen atom interacts with a tin atom.
[b] For this coverage, the Sn–O bond is long (2.8 Å) and the η_3Sn *cis* mode looks like a di-σ_{CC} one.
[c] With 8 layers of vacuum between slabs.

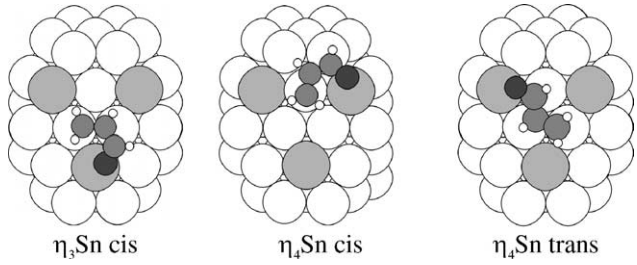

Fig. 5. Top and side views of the most stable adsorption modes of acrolein on the p(2 × 2) Pt_3Sn alloy (see Fig. 1 for labels of spheres).

The energy results are given in Table 3. The most stable mode for acrolein at a coverage of 1/12 remains the η_3Sn *cis* one followed by the two η_4Sn modes instead of the di-σ_{14} mode which was the second most stable on the $(\sqrt{3} \times \sqrt{3})R30°$ alloy. If the adsorption energies of the η_3 *cis* and η_4 *cis* modes are compared with those of the η_3Sn *cis* and η_4Sn *cis* modes, a stabilization of 7 kcal/mol is observed when the oxygen atom interacts with tin instead of platinum. This is a measure of the strength of the Sn–O bond compared to the Pt–O bond. The most stable modes are represented in Fig. 5. The η_3Sn *cis* mode looks like that on the first alloy, but we can describe more precisely the η_4 modes: the η_4Sn *cis* geometry is a combination of a π_{CC} and a di-σ_{CO} modes while the η_4Sn *trans* one is a combination of a di-σ_{CC} and a di-σ_{CO} modes. The behavior of prenal is the same on both alloys: the atop-Sn mode is the sole significantly stable one.

For acrolein, a higher coverage has also been considered ($\theta = 1/4$) giving a (2 × 2) adsorbate arrangement. Only the best adsorption modes have been calculated. The η_3Sn *cis* mode remains the most stable although it is slightly destabilized compared to coverage 1/12. In this geometry, the SnO bond is long (2.8 Å), which means that the interaction

is weak. Nevertheless this form does not evolve by a further decoordination of the oxygen to the di-σ_{CC} one which is less stable. The same phenomenon as on Pt(111) is observed: the di-σ_{CC} modes are more stable than at lower coverage. We have explained this result by the existence of stabilizing lateral dipole–dipole interactions induced by the presence of oxygen in the molecules. The η_4Sn *trans* geometry, involving four surface atoms, is more strongly destabilized and the η_4Sn *cis* geometry even transforms to the η_3Sn *cis* one, even if this transformation needs an important movement from π_{CC} to di-σ_{CC}. Obviously, prenal remains atop at high coverage.

In conclusion, the two alloys have roughly the same behavior toward the adsorption of the studied unsaturated aldehydes, although, in some aspects, the Pt_3Sn alloy is intermediate between Pt and Pt_2Sn. The same adsorption modes are observed, except the η_4Sn *trans* one which does not exist in the case of the $(\sqrt{3}\times\sqrt{3})R30^\circ$ Pt_2Sn alloy. There is also a slight difference in the stability order since the di-σ_{14} geometry is the second most stable for Pt_2Sn against the η_4Sn geometries in the case of Pt_3Sn.

6. Discussion

In this section we will compare the results obtained for the two studied alloys with those obtained for Pt(111) and described in [19]. Then we will try to relate the adsorption behavior of the unsaturated aldehydes on Pt(111) and on its alloys with tin to the selectivity of their hydrogenation.

6.1. Comparison of the adsorption on Pt(111) and on the two Pt–Sn alloys and electronic interpretation

In the case of the p(2 × 2) Pt_3Sn alloy, we can compare the di-σ_{CC}, the η_3 *cis*, and η_4 *cis* modes, which also exist on Pt(111). For a coverage of 1/12 in the case of acrolein, we note a decrease of the adsorption energy of 8.9, 12.2, and 12.5 kcal/mol on the alloy for these three modes, respectively. In the case of the $(\sqrt{3}\times\sqrt{3})R30^\circ$ Pt_2Sn alloy, only the di-σ_{CC} and the π_{CC} *cis* and *trans* can be compared, the η_3 or η_4 modes involving a Sn atom. A decrease of 10.7, 6.5, and 6.5 kcal/mol is observed for the three modes, respectively. Hence the π_{CC} modes are less destabilized than the di-σ_{CC}. For crotonaldehyde and prenal also, the adsorption energy decreases strongly from Pt to Pt_2Sn(111) for the geometries parallel to the surface. Such a decrease of the alkene adsorption energy has been observed experimentally on these two alloy surfaces [15–17], although its value is smaller (4 kcal/mol for Pt_3Sn and 6 kcal/mol for Pt_2Sn). Recent periodic DFT calculations for ethylene on Pt(111), Pt_3Sn(111) [25], and cluster calculations [24] give the same trend. We have seen in the previous section that the atop-Pt modes are not stable on the Pt_2Sn alloys, whereas they are stable on Pt(111) (−6, −6.3, and −8.3 kcal/mol for acrolein, crotonaldehyde, and prenal, respectively). On the other hand, the atop-Sn geometries are stable, particularly for crotonaldehyde and prenal, which again highlights the better interaction of the oxygen atom with tin compared to platinum. They are nevertheless less stable than the corresponding atop-Pt modes on pure platinum.

We have already pointed out previously that the η_3Sn *cis* and η_4Sn *cis* modes are also stabilized by this Sn–O interaction compared to the η_3 *cis* or η_4 *cis* modes. As a result, the additional adsorption energies for the η_3Sn *cis* or η_4Sn *cis* modes compared to the di-σ_{CC} ones are larger on the alloy than on platinum: for acrolein 4.4 vs 1.7 kcal/mol, and for crotonaldehyde 3.9 vs 1.1 kcal/mol. This important Sn–O interaction explains also the existence of the di-σ_{14} geometry, where the oxygen atom interacts with tin by its lone pair. Nevertheless, these modes involving a Sn atom are less stable than the corresponding modes on pure platinum, which shows that the specific interaction of oxygen with Sn does not fully compensate the weakening of the Pt–C interactions on the alloy.

In summary, all the adsorption modes on the alloy are less strongly bound than on platinum. A recent study deals with the hydrogenation of crotonaldehyde over the two Pt–Sn alloys studied in the present paper [39]. It is found that the reactivity is enhanced on the alloys, which could be related to the weaker adsorption, although a complete study of the reaction pathways would be needed to assess this.

The variation of the adsorption energies when platinum is alloyed with tin can be easily understood by the consideration of the electronic structure of the alloys. We have seen in Section 3 that an electron transfer occurs from Sn to Pt. It results in a large positive charge on the Sn atoms which can be considered as $Sn^{\delta+}$. On the contrary, the surface Pt atoms are more negatively charged on the alloy than on pure platinum. An alkene being mainly an electron donor, its interaction with the electron-enriched Pt atoms of the surface is weakened. This can be seen as an increased Pauli repulsion between the π electrons of the alkene and the d electrons of the surface Pt atoms. One can also understand that the electron-rich oxygen atoms have a better interaction by their lone pairs with the depleted Sn atoms than with the Pt atoms. It is also easy to explain why the double bonds, either C=C or C=O, do not adsorb favorably on sites containing a Sn atom. Effectively, the filled d-band of Sn is too low in energy to give rise to back-donation and the sp band, which is partially empty, takes part only slightly in this interaction. The decrease of the back-donation compared to Pt is not compensated by the increase of the donation of the occupied π orbitals to the vacant Sn orbitals and therefore the tin atoms are not favorable sites for the adsorption of double bonds.

The molecule–surface interaction processes can be described in more details from an analysis of the DOS. We have also pointed out in Section 3 that the shape of the DOS changes with alloying and that the d-band center is displaced farther from the Fermi level. Let us consider the di-σ_{CC} adsorption mode of acrolein on Pt and Pt_2Sn. The main interactions occur between the π orbitals of acrolein located

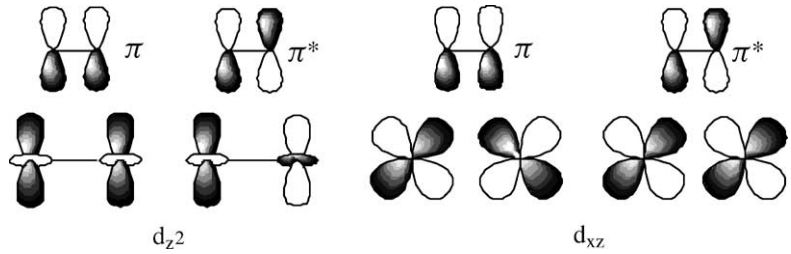

Scheme 2. Schematic interactions between the orbitals of the surface Pt atoms and the π system of acrolein in the di-σ_{CC} geometry.

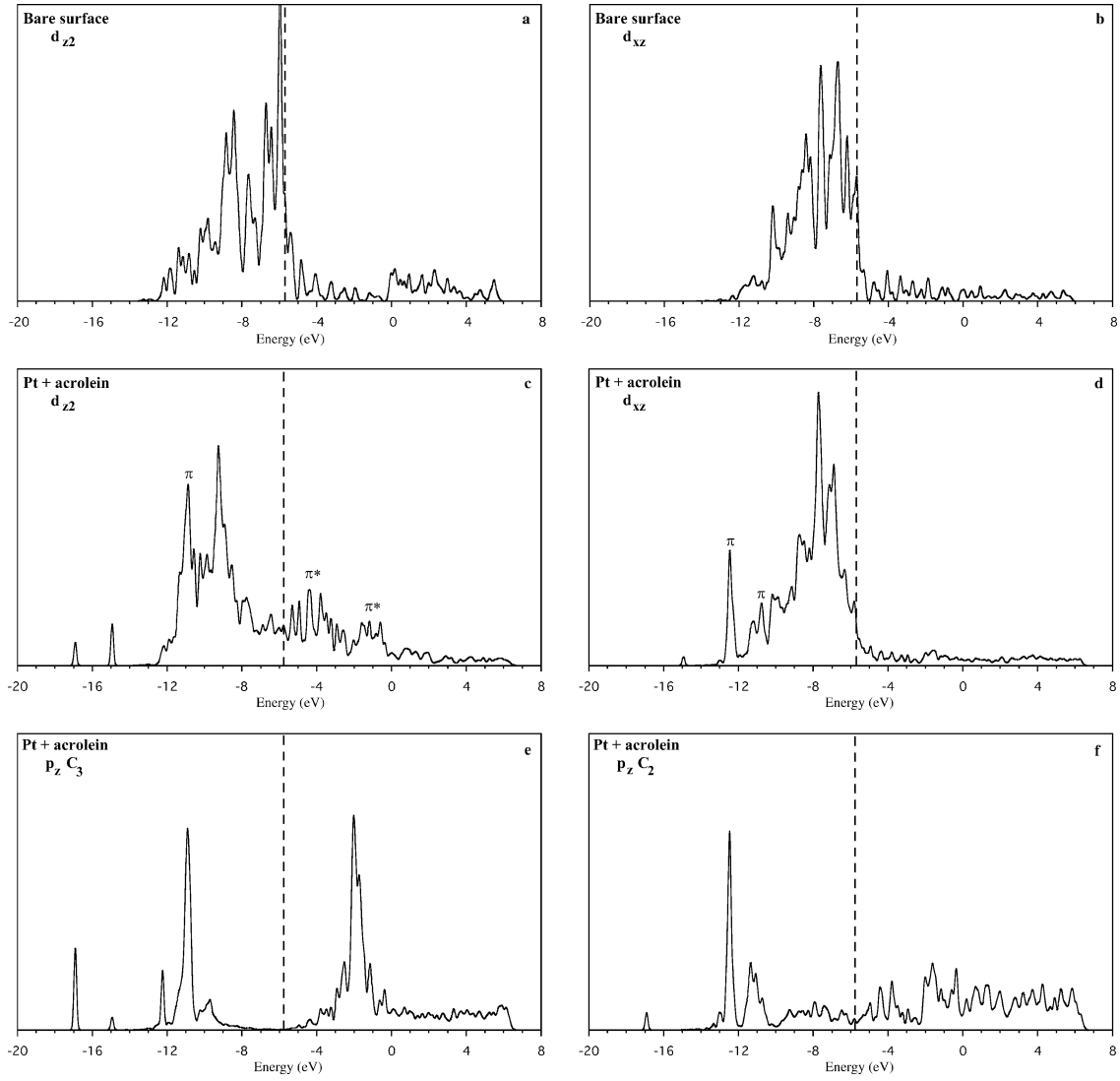

Fig. 6. di-σ_{CC} adsorption mode of acrolein on Pt(111), DOS-projected on the d_{z^2} and d_{xz} orbitals of an interacting surface Pt atom: (a, b) on the bare surface; (c, d) after adsorption; DOS-projected on the C_2 and C_3 carbons of acrolein. The numbering of the acrolein atoms is shown in Table 1. The dashed line indicates the Fermi level.

on C_1 and C_2 and the d_{z^2} and d_{xz} orbitals of the two platinum atoms involved in the adsorption (see Scheme 2). The DOS projected on the interacting orbitals d_{z^2} and d_{xz} of the Pt atoms and on the p_z orbitals of the C_2 and C_3 carbon atoms are plotted on Figs. 6 and 7 for the cases of Pt and Pt_2Sn, respectively (for the numbering of the carbon atoms, see Table 1). In these figures, the DOS have all the same energy reference (energy of vacuum). Acrolein has four π orbitals: two occupied $\pi_{CC} + \pi_{CO}$ and $\pi_{CC} - \pi_{CO}$ and two vacant $\pi^*_{CC} + \pi^*_{CO}$ and $\pi^*_{CC} - \pi^*_{CO}$. In the gas phase, all atoms have contributions in the four orbitals. In the adsorbed di-σ geometry, the molecule is distorted and the two π systems are more separated. Moreover the π system mixes with the σ one, which gives more numerous peaks. The combination

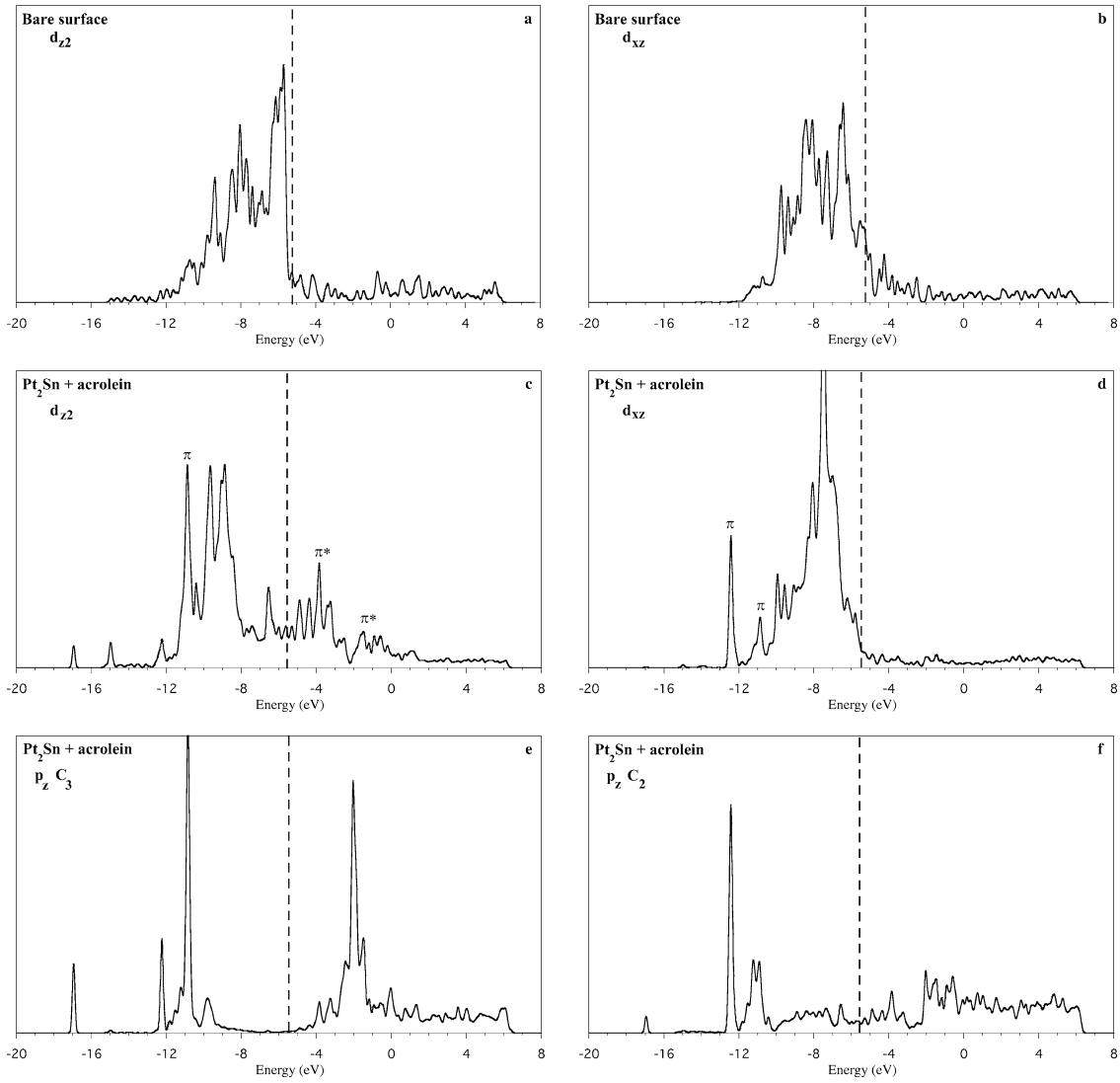

Fig. 7. di-σ_{CC} adsorption mode of acrolein on $Pt_2Sn(111)$, DOS-projected on the d_{z^2} and d_{xz} orbitals of an interacting surface Pt atom: (a, b) on the bare surface; (c, d) after adsorption; DOS-projected on the C_2 and C_3 carbons of acrolein. The numbering of the acrolein atoms is shown in Table 1. The dashed line indicates the Fermi level.

of the DOS projected on the p_z orbitals of carbons C_2 and C_3 (Figs. 6e and f) allows us to assign the peaks around -12.5 and -10.9 eV to the π orbitals of acrolein. These peaks are widened, particularly the latter (Fig. 6f), which indicates the existence of an interaction with the Pt orbitals. The π^* orbitals appear as two large bands between the Fermi level and -2.5 eV and between -2.5 and 0 eV, with a large contribution of p_z C_3 at -2 eV. This broadening also shows an important interaction with the Pt orbitals.

If the DOS projected on d_{z^2} in the case of bare Pt and in the case of the acrolein adsorption are compared (Figs. 6a and c), one observes that a large part of the d-band has been pushed above E_F. There are two possible reasons. The first one is the repulsive four-electron interactions of Pauli type between the occupied π orbitals and the almost full d-band of platinum, which stabilize the π orbital and destabilize the d-band. The peak at -10.9 eV, corresponding to the π system of acrolein, reflects this interaction. The second reason is the back-donation from the d-band to the π^* orbitals of acrolein, the antibonding combination of which appears above E_F. Hence, the two large bands between the Fermi level and the 0 eV correspond to interactions of d_{z^2} with both π and π^*. Similarly, in the DOS projected on d_{xz} (Fig. 6d), one observes a high peak at -12.5 eV and small peaks between -11.5 and -10.5 eV (by comparison with Fig. 6b) corresponding also to the π system of acrolein. For d_{xz}, the interaction with the π^* orbital is weak: one can only observe a small peak around -2 eV. In this case, no shift of the d-band above E_F is observed.

In the case of the alloy, the same features are observed (Fig. 7). The d_{z^2} orbital also shows a large part above the Fermi level. Peaks at -12.4 (d_{xz}) and -10.9 (d_{z^2} and d_{xz}) show the interaction with the π orbitals of acrolein. It is difficult to compare the strength of the interactions between the

d and the π orbitals since no significant displacement is observed for the latter between the case of pure platinum and the case of the alloy. Hence we cannot see the stronger repulsive four-electron interactions which would be induced for the alloy by the lower d-band center. In contrast, the π^* orbital located at -2 eV in the case of Pt (Fig. 6e) is downshifted to -2.5 eV in the case of Pt_2Sn (Fig. 7e). Moreover this orbital is broader in the case of Pt (Fig. 6e compared to Fig. 7e). These two observations suggest a better interaction of the d orbitals with π^* in the case of Pt, in agreement with the higher d-band center.

The weaker interaction of the Pt orbitals with π^* stabilizes less the d-band in the alloy case. Moreover, the stronger interaction of the Pt orbitals with π destabilizes more the d-band. The two effects result in a smaller displacement of the d-band center upon adsorption in the case of the alloy. Indeed, in both cases (Pt and Pt_2Sn) the d-band is pushed farther from E_F after adsorption. The d-band center is calculated at -2.20 eV for Pt and -2.27 eV for Pt_2Sn, with respect to the Fermi level, compared to -1.93 and -2.12 eV, respectively, in the case of the clean surfaces. Hence the d-band center moves much more in the case of Pt (-0.27 eV) than in the case of Pt_2Sn (-0.15 eV). All the previous arguments converge to the conclusion that the adsorption of acrolein in the di-σ_{CC} geometry is weaker on the alloy than on platinum. This can also be related to the geometrical parameters. Indeed, the Pt–C bonds are longer on the alloy, 2.143 and 2.177 Å vs 2.124 and 2.155 Å on platinum and the C=C bond is less elongated on the alloy, 1.479 vs 1.483 Å.

Besides the change of the adsorption energies, a marked change in the preferred adsorption modes is observed when the two surface alloys are compared with platinum. On Pt(111) at low coverage (1/9 or 1/12), all three aldehydes prefer geometries involving the whole molecule (η_3 *cis* or η_4 *trans* for acrolein and crotonaldehyde, η_4 *trans* for prenal) [19]. Acrolein on the alloys still prefers this type of modes, η_3 *cis* on both alloys. The behavior of crotonaldehyde and prenal is different. For crotonaldehyde, the η_3 *cis* mode is also the most stable but numerous other modes are not far in energy, among them the atop-Sn one. For prenal only the atop-Sn mode can be considered as stable. The difference is then more pronounced in the case of prenal for which the atop-Pt mode becomes the most stable on pure platinum only at high coverage ($> 1/6$).

At high coverage, the behavior of acrolein changes compared with platinum. On the Pt_2Sn alloy, the di-σ_{14} mode is the most stable one. Moreover, already at coverage 1/6, the modes parallel to the surface (η_3 and η_4) do no more exist and transform into di-σ_{CC} or π_{CC} modes (Table 2). On Pt(111), these modes still remain stable at this coverage and even at a coverage of 1/4, although less stable than the di-σ_{CC} modes. On Pt_3Sn at coverage 1/4, the modes parallel to the surface are less destabilized since η_4Sn *trans* still exists, although not very stable (Table 3). The η_3Sn *cis* mode does not transform totally into di-σ_{CC} *cis* since the oxygen atom remains directed toward the surface at a long distance (Sn–O = 2.8 Å). Nevertheless, it can be considered as a di-σ_{CC} mode, the interaction between Sn and O being weak. In conclusion, at high coverage, acrolein is di-σ_{14} in competition with di-σ_{CC} on Pt_2Sn ($\theta = 1/6$) and di-σ_{CC} on Pt_3Sn ($\theta = 1/4$).

Table 4
Experimental selectivity to saturated aldehyde (SAL), unsaturated alcohol (UOL), and saturated alcohol (SOL) during the hydrogenation of unsaturated aldehydes on Pt/aerosil and PtSn/aerosil (from Ref. [3])

	SAL		UOL		SOL	
	Pt	PtSn	Pt	PtSn	Pt	PtSn
Acrolein	92.6	67.0	1.6	27.5	1.8	2.9
Crotonaldehyde	50.0	50.1	13.0	29.5	33.6	19.4
Prenal	17.0	7.6	20.5	77.5	55.0	14.9

Crotonaldehyde behaves similarly to acrolein: at high coverage (1/6), the di-σ_{14} and di-σ_{CC} modes are in competition. Prenal, which is already atop at low coverage, is a fortiori also atop at high coverage.

We have therefore just seen that the unsaturated aldehydes have a different adsorption behavior on platinum and on its alloy with tin. We will now show that there is a relation with the different selectivity observed during the hydrogenation of these aldehydes on Pt and the Pt–Sn alloys.

6.2. Relation between adsorption and hydrogenation selectivity

First we recall here some experimental results (see Table 4). On silica-supported Pt catalysts, an increase of the selectivity to unsaturated alcohol (UOL) is observed when going from pure Pt to Pt–Sn alloys: from 2 to 27% for acrolein, from 13 to 29% for crotonaldehyde, and from 20 to 77% for prenal, at low conversion. The concomitant decrease in the quantity of saturated alcohol (SOL) in the case of the alloy must be underlined: from 34 to 19% for crotonaldehyde and from 55 to 15% for prenal. That means that on Pt–Sn, only a small quantity of SOL is formed as primary product of the reaction, if any, or the further hydrogenation of UOL is difficult, in contrast to the case on pure platinum. Obviously, the fact that the experiments are performed with supported catalysts makes more difficult the direct comparison with our calculations. In the study cited above which deals with the hydrogenation of crotonaldehyde over the two Pt–Sn alloys studied in the present work [39], the conclusion is that the selectivity does not change much on the alloy compared to platinum.

The case of prenal is the simplest one: even at low coverage, the atop mode is the most stable and leads to the C=O hydrogenation (UOL). On pure platinum, this mode becomes the most stable only at high coverage. The absence of the η_4 modes for PtSn precludes the formation of the saturated alcohol SOL as primary product, as it is the case on platinum. Moreover we have considered the further behavior of the unsaturated alcohol formed, the 3-methyl-2-butenol. Like for prenal, the atop-Sn mode is the most stable with an

adsorption energy of −7.6 kcal/mol, the di-σ_{CC} mode being 5 kcal/mol less stable. The preferred adsorption in the atop geometry precludes the hydrogenation of the C=C bond and hence the obtention of SOL. The situation is totally different on platinum, on which 3-methyl-2-butenol adsorbs in the di-σ_{CC} geometry and is easily hydrogenated to SOL. Hence Pt and Pt–Sn have a the different behavior toward the second hydrogenation reaction.

The cases of acrolein and crotonaldehyde are less clear. At low coverage, the best adsorption geometry is the η_3 *cis* one, like on platinum, which leads to the C=C hydrogenation (SAL). At higher coverage, the di-σ_{14} becomes in competition with the di-σ_{CC} one. Hence the greatest part of acrolein and crotonaldehyde is hydrogenated through the C=C bond (SAL) as on platinum. However, the behavior of the di-σ_{14} geometry toward hydrogenation is not known. Does this mode lead to the hydrogenation of the C=C or of the C=O bond? This will be actually the subject of a forthcoming study.

Several experimental studies assume that the active species of the Pt–Sn alloys, responsible for the enhanced catalytic properties, are not the Sn atoms but rather tin oxides SnO_x formed at the surface [11, and references therein], [40]. These oxides act as Lewis acids and coordinate to the oxygen atom of the aldehydes, leading to a polarization of the C=O bond and hence to an easier hydrogenation of this bond. Nevertheless, another author noted that the bimetallic Pt–Sn/SiO_2 catalysts in which Sn^0 atoms are present are more selective toward the unsaturated alcohol than those containing ionic tin Sn^{IV} or Sn^{II} present as oxidized species [41].

Our results show that, effectively, it is not necessary to oxidize Sn in order to have coordination by the oxygen atom. This is due to the fact that there is an electron transfer in the alloy from the Sn atoms to the Pt ones (vide Section 3), which leads to positively charged Sn atoms. We have nevertheless investigated the influence of oxidized tin on the adsorption of acrolein on the Pt_2Sn alloy. For that we have adsorbed one oxygen per unit cell (coverage 1/9) on sites containing a tin atom. We have compared the adsorption atop on a tin atom, bridge between a tin and a platinum atoms and three-fold between a tin and two platinum atoms. The most stable structure is the fcc threefold one. It is more stable than the hcp threefold one by 6.3 kcal/mol. The bridge site does not exists and evolves to the threefold fcc one. The atop site is far less stable. These results are in agreement with previous calculations [25]. We have then studied the adsorption of acrolein on the surface containing one fcc threefold oxygen, the adsorption geometries involving the oxidized Sn atom. The η_3Sn *trans* mode evolves into the di-σ_{CC} *trans*, with a slightly smaller adsorption energy than on the nonoxidized surface. The η_4Sn *cis* geometry evolves into the η_3Sn *cis* one, which is 4 kcal/mol less stable than on the nonoxidized surface. The most stable mode is the di-σ_{14} one. Its adsorption energy is increased by 0.9 kcal/mol compared with the nonoxidized surface. The atop-Sn mode is also more stable by 2.9 kcal/mol. Hence the modes involving a real Sn–O single bond (atop and di-σ_{14}) are slightly stabilized on the oxidized surface. Moreover, in the case of acrolein, the best adsorption mode in changed from η_3Sn *cis* to di-σ_{14} when the surface is oxidized. Therefore the presence of oxidized tin atoms increases the stability of the atop-Sn mode relative to the other modes. For crotonaldehyde it becomes competitive with the di-σ_{14} and the η_3Sn *cis* modes and for prenal its predominance is accentuated. Hence the better yield in UOL for crotonaldehyde and prenal on the alloy can be explained by the presence of oxidized tin atoms, although, in the case of prenal, this effect is already present without oxidation. In the case of acrolein for which the di-σ_{14} mode is the most stable, the reactivity of this mode should be known in order to conclude, as pointed out before.

7. Conclusion

Although the adsorption structures of the adsorbate might not be the only important factor for the determination of the hydrogenation selectivity, the present study shows that the knowledge of such structures allows us to give a qualitative interpretation of the reactivity trends. DFT calculations are a useful tool for obtaining information on the factors which can change the adsorption geometries.

In this study, we have particularly compared the adsorption geometries of the unsaturated aldehydes on platinum and on two Pt–Sn alloys, in order to understand why the selectivity of their hydrogenation toward unsaturated alcohol is enhanced on the alloys especially for prenal. In all cases, the adsorption energy is smaller on the alloys than on platinum, which could explain the enhancement of the reactivity observed experimentally. Effectively, the activity of ethylene hydrogenation is increased by 75% with PtSn catalysts [42], and so does also that of crotonaldehyde hydrogenation [39].

One observes on the alloys an enhancement of the relative stability of the atop-Sn mode, where the molecule interacts by the oxygen atom, comparatively to the other modes. For prenal it is the most stable modes at all coverages, which explains the high yield in unsaturated alcohol. For acrolein and crotonaldehyde, the η_3 *cis* mode and the di-σ_{CC} mode remain the most stable on the alloy, which gives a high yield in saturated aldehyde, as on platinum. Nevertheless the di-σ_{14} mode becomes competitive at lower coverage, which could explain why more unsaturated alcohol is obtained compared to platinum, if this mode leads to the hydrogenation of the C=O bond. This assumption must be verified by the study of the reaction path.

The second hydrogenation (hydrogenation of the formed unsaturated alcohol) does not take place on the alloys as it does on platinum, due to the fact that UOL adsorbs atop-Sn and not di-σ_{CC}, hence with no activation of the C–C bond.

The presence of oxidized tin atoms accentuates the preference for the atop-Sn mode for prenal and crotonaldehyde, which agrees with the increase of the selectivity to UOL, but

gives a preference for the di-σ_{14} mode in the case of acrolein, the evolution of which is not known. In the case of prenal, however, the oxidation of tin is not necessary for explaining the selectivity.

The different behavior of the alloys compared to platinum has been explained in terms of interactions between the d-band of the surface platinum atoms and the π and π^* orbitals of the substrate, in relation to the shape of the DOS and the movement of the d-band center. The interactions of the d-band with π^* are weaker on the alloys and, on the contrary, the repulsive Pauli interactions are stronger, which results in a smaller adsorption energy for the modes involving the C=C bond. This phenomenon has a strong influence on the molecular chemisorption mode and on the related hydrogenation selectivity.

Acknowledgments

The authors thank the Institut du Développement et des Ressources en Informatique Scientifique (IDRIS) at Orsay (Project 609) and the Centre Informatique National de l'Enseignement Supérieur (CINES) at Montpellier for CPU time.

References

[1] S. Galvagno, Z. Poltarzewki, A. Donato, G. Neri, R. Pietropaolo, J. Mol. Catal. 35 (1986) 365.
[2] Z. Poltarzewki, S. Galvagno, R. Pietropaolo, P. Staiti, J. Catal. 102 (1986) 190.
[3] T.B.L.W. Marinelli, S. Nabuurs, V. Ponec, J. Catal. 151 (1995) 431.
[4] V. Ponec, Appl. Catal. A 149 (1997) 27.
[5] G.F. Santori, M.L. Casella, G.J. Siri, H.R. Aduriz, O.A. Ferretti, Appl. Catal. A 197 (2000) 141.
[6] F. Coloma, A. Sepulveda-Escribano, J.L.G. Fierro, F. Rodriguez-Reinoso, Appl. Catal. A 148 (1996) 63.
[7] F. Coloma, A. Sepulveda-Escribano, J.L.G. Fierro, F. Rodriguez-Reinoso, Appl. Catal. A 136 (1996) 231.
[8] A.B. da Silva, E. Jordão, M.J. Mendes, P. Fouilloux, Appl. Catal. A 148 (1997) 253.
[9] M. English, V.S. Ranade, J.A. Lercher, J. Mol. Catal. A 121 (1997) 69.
[10] J.L. Margitfalvi, A. Tompos, I. Kolosova, J. Valyon, J. Catal. 174 (1998) 246.
[11] N. Homs, J. Llorca, P. Ramirez de la Piscina, F. Rodriguez-Reinoso, A. Sepulveda-Escribano, J. Silvestre-Albero, Phys. Chem. Chem. Phys. 3 (2001) 1782.
[12] M.T. Paffett, S.C. Gebhard, R.G. Windham, B.E. Koel, J. Phys. Chem. 94 (1990) 6831.
[13] C. Xu, B.E. Koel, Surf. Sci. Lett. 304 (1994) L505.
[14] C. Xu, B.E. Koel, Surf. Sci. 310 (1994) 198.
[15] M.T. Paffett, S.C. Gebhard, R.G. Windham, B.E. Koel, Surf. Sci. 223 (1989) 449.
[16] Yi-Li. Tsai, C. Xu, B.E. Koel, Surf. Sci. 385 (1997) 37.
[17] Yi-Li. Tsai, B.E. Koel, J. Phys. Chem. B 101 (1997) 2895.
[18] D. Stacchiola, S. Azad, L. Burkholder, W.T. Tysoe, J. Phys. Chem. B 105 (2001) 11233.
[19] F. Delbecq, P. Sautet, J. Catal. 211 (2002) 398.
[20] S. Pick, Surf. Sci. 436 (1999) 220.
[21] M.-S. Liao, C.R. Cabrera, Y. Ishikawa, Surf. Sci. 445 (2000) 267.
[22] J.A. Rodriguez, S. Chaturvedi, T. Jirsak, J. Hrbek, J. Chem. Phys. 109 (1998) 4052.
[23] J.A. Rodriguez, T. Jirsak, S. Chaturvedi, J. Hrbek, J. Am. Chem. Soc. 120 (1998) 11149.
[24] J. Shen, J.M. Hill, R.M. Watwe, B.E. Spiewak, J.A. Dumesic, J. Phys. Chem. B 103 (1999) 3923.
[25] R.W. Watwe, R.D. Cortright, M. Mavrikakis, J.K. Norskov, J.A. Dumesic, J. Chem. Phys. 114 (2001) 4663.
[26] A.N. Haner, P.N. Ross, U. Bardi, in: S.Y. Tong, M.A. van Hove, K. Takayanagi, X.D. Xie (Eds.), Springer Series in Surface Science—The Structure of Surfaces III, Vol. 24, Springer, Berlin, 1991.
[27] A. Atrei, U. Bardi, G. Rovida, M. Torrini, E. Zanazzi, P.N. Ross, Phys. Rev. B 46 (1992) 1649.
[28] Y. Li, B.E. Koel, Surf. Sci. 330 (1995) 193.
[29] M.T. Paffett, R.G. Windham, Surf. Sci. 208 (1989) 34.
[30] S.H. Overbury, D.R. Mullins, M.T. Paffett, B.E. Koel, Surf. Sci. 254 (1991) 45.
[31] A. Atrei, U. Bardi, J.X. Wu, E. Zanazzi, G. Rovida, Surf. Sci. 290 (1993) 286.
[32] M. Galeotti, A. Atrei, U. Bardi, G. Rovida, M. Torrini, Surf. Sci. 313 (1994) 349.
[33] G. Kresse, J. Hafner, Phys. Rev. B 47 (1993) 558.
[34] G. Kresse, J. Hafner, Phys. Rev. B 48 (1993) 13115.
[35] G. Kresse, J. Hafner, Phys. Rev. B 49 (1994) 14251.
[36] J.P. Perdew, Y. Wang, Phys. Rev. B 45 (1992) 13244.
[37] R.G. Pearson, Inorg. Chem. 27 (1988) 734.
[38] M. Batzill, D.E. Beck, B.E. Koel, Surf. Sci. 466 (2000) L821.
[39] D.I. Jerdev, A. Olivas, B.E. Koel, J. Catal. 205 (2002) 278.
[40] T.B.L.W. Marinelli, V. Ponec, J. Catal. 156 (1995) 51.
[41] P. Claus, Top. Catal. 5 (1998) 51.
[42] Y.-K. Park, F.H. Ribeiro, G.A. Somerjai, J. Catal. 178 (1998) 66.